applied optics

Liquid index matching for 2D and 3D terahertz imaging

J. B. PERRAUD,[1,2] J. BOU SLEIMAN,[1] B. RECUR,[3] H. BALACEY,[3] F. SIMOENS,[2] J. P. GUILLET,[1] AND P. MOUNAIX[1,*]

[1]Bordeaux University, IMS, CNRS UMR 5218, 351 Cours de la Libération 33405 Talence, France
[2]CEA - LETI Direction de la Recherche Technologique, 17 Rue des Martyrs, 38054 Grenoble Cedex 9, France
[3]Noctylio SAS, 59 Cours de l'Intendance, 33000 Bordeaux, France
*Corresponding author: patrick.mounaix@u-bordeaux.fr

Received 21 June 2016; revised 8 September 2016; accepted 11 October 2016; posted 11 October 2016 (Doc. ID 268695); published 8 November 2016

Two-dimensional (2D) terahertz imaging and 3D visualization suffer from severe artifacts since an important part of the terahertz beam is reflected, diffracted, and refracted at each interface. These phenomena are due to refractive index mismatch and reflection in the case of non-orthogonal incidence. This paper proposes an experimental procedure that reduces these deleterious optical refraction effects for a cylinder and a prism made with polyethylene material. We inserted these samples in a low absorption liquid medium to match the sample index. We then replaced the surrounding air with a liquid with an optimized refractive index, with respect to the samples being studied. Using this approach we could more accurately recover the original sample shape by time-of-flight tomography.

OCIS codes: (100.6950) Tomographic image processing; (110.6795) Terahertz imaging; (110.6955) Tomographic imaging; (100.3010) Image reconstruction techniques; (300.6495) Spectroscopy, terahertz.

http://dx.doi.org/10.1364/AO.55.009185

1. INTRODUCTION

Terahertz (THz) and millimeter waves penetrate various dielectric materials, including plastics, ceramics, and crystals, permitting the consideration of THz transmission and reflection images. Terahertz imaging is now a well-established technique in various applications as an industrial, nondestructive method that can be used to analyze geometrically complex objects [1–5]. Tomographic techniques can also be used to recover three-dimensional (3D) images in the THz frequency range, in the same way they are applied in the optical, infrared, or x-ray ranges of the electromagnetic spectrum. Some of these techniques have been specifically developed to visualize the shape of 3D objects [6,7]. Measuring the time of flight of the reflected THz pulses with a time domain terahertz system, for example, can reveal the inner structures of a multilayered flat object [8–11].

For nonplanar objects like cylinders, however, different effects appear in THz imaging, depending on the angular positions of the projection. We noticed the lens effect at the center of the projection of a cylinder, but observed a strong diffraction effect for radial positions. The first effect induces higher pixel values at the core of the cylinder while the second one makes the cylinder larger. Artifacts are consequently induced in the volume reconstruction. As a result, the rebuilt cylinder image is oversized when tomography algorithms are executed. The refractive index mismatch creates severe refraction effects at the interfaces [12]. In addition, the THz radiation amplitude value measured by the sensors depends on the beam deviation induced by refractive index mismatch, coupled with the absorption properties of the sample. Generally, the medium around the sample is air, with a refractive index close to unity that generally differs significantly from the sample refractive index.

When numerical computation is applied, the back-projection algorithm hypothesis assumes that diffraction effects and Fresnel losses are negligible since the beam trajectory is supposedly straightforward [13]. In practice, the THz beam is significantly affected by the Fresnel effect, even with low refractive index materials, inducing artifacts on 2D images. To reduce these effects, we propose the sample to be inserted in a liquid medium with an optimized refractive index. This idea is not new in optics. For example, an index-matching material is a substance, usually a liquid or even a gel, that presents a refraction index at the working wavelength that matches the index of another item, such as a lens, material, or fiber optic. In that case, if the two substances with similar indexes are close enough or in contact, the beam will travel from one to the other without reflection or refraction. We propose to demonstrate that concept in the case of THz imaging and our results successfully illustrate an improvement in THz imaging, in particular providing better 3D inspection accuracy and dimensional measurements from volume and surface rendering.

2. EXPERIMENT

We used a TPS Spectra 3000 from Teraview for our experiments. It was a standard THz-TDS transmission setup based on a mode-locked Ti:sapphire laser providing 80 fs pulses with a 76 MHz repetition rate. Typically, this instrument's useful bandwidth range was between 0.1 and 4.5 THz, depending on the investigated sample. We split the laser output into the pump and probe beams and focused the pump onto a photoswitch to generate the THz field. This field was transmitted through the sample and was finally detected by a photoswitch triggered by the probe laser beam. Upon its interaction with the sample, we measured the time-resolved field variation using a variation in the photocurrent induced by the probe laser beam into the detector made of a LT-GaAs semiconductor. Finally, we filtered out and amplified the photocurrent induced by the probe laser beam.

We used a time delay line to sample the signal step by step and then rebuilt the THz field using the sampling technique. To minimize noise effects, all the signals we processed in this study corresponded to an average of 50 acquisitions. We conducted the measurements under dry air. A hygrometer controlled the relative humidity level in real time and kept it below 1% by using a flow of dry air. We performed this control in real time by monitoring two spectral lines of water vapor at 1.12 and 1.7 THz on the reference spectrum. This TDS system offers a useful frequency range of 0.2–3 THz with a maximum dynamic range around 75 dB, a spectral resolution of 0.06 THz, and a rapid scan mode at the rate of 30 scans/s. For the transmission setup, we placed the sample at the focal point of the THz radiation, midway between two off-axis parabolic mirrors described in Fig. 1. We used a (X, Y) translating stage positioned in the plane of the sample to perform a raster scanning with a maximum area of 16 mm × 16 mm, which gave access to spectral images in the focal plane (X, Y) after signal conversion from the temporal to the frequency domain. The precision of the displacement stage was 0.1 μm.

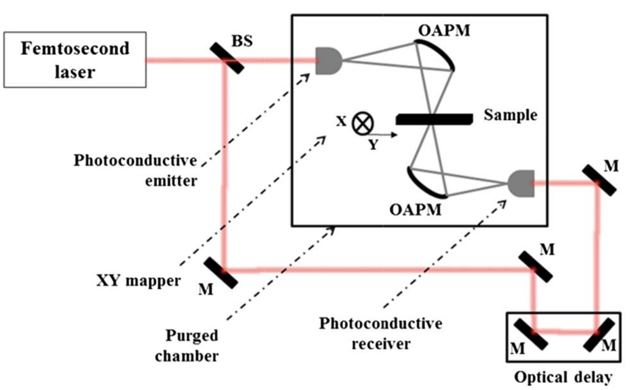

Fig. 1. Schematic of the setup in the transmission mode (OAPM, off axis parabolic mirror; BS, beam splitter; M, mirror).

3. METHOD

Dielectric properties of pure and mixture liquids in the terahertz frequency range have been the subject of much research in the scientific community [14,15]. Such investigations have provided valuable information on the relaxation processes of molecules and their intermolecular responses after interaction with a THz pulse. Induced dipole interaction into nonpolar liquid has resulted in a low absorption coefficient up to several THz [16]. In this work, we focusses on nonpolar liquid n alkanes because of their notable dielectric properties. This chemical compound, C_nH_{2n+2}, with n equal to the number of carbon atoms, presented a very useful dielectric response that varied with the number of carbon atoms in their linear chain [17]. Liquid alkanes, for example, presented a flat optical dispersion curve from 100 GHz up to several THz. This is a welcome feature for index matching since we can observe a monotonic variation of the index from 1.35 up to 1.43. The absorption coefficients of these nonpolar liquids, arising from transient induced dipoles, are essentially featureless in this spectral range, with an almost linear dependence on frequency, negligible temperature dependence, and values less than 1 cm^{-1} [17]. On the contrary, the optical index varies with temperature so we can thermally tune the index to optimize the index-matching condition.

The experimental procedure consisted of three consecutive acquisitions for each sample of index- matching material [18]: (i) the reference signal waveform of the spectrometer without a PE cell to contain the liquid in the sample compartment, (ii) the waveform of the empty cell that will be filled with liquid, and, (iii) the waveform with the cell filled with the liquid being investigated. Measurements (i) and (ii) were used to accurately determine the dielectric properties of the cell, which was made of high-density polyethylene (HDPE).

We used measurements (ii) and (iii) to characterize the liquid. Then, the THz-TDS allowed us to determine the complex optical index $n^* = n + jk$, where n is the optical index and k is the extinction coefficient. We selected liquid paraffin, also known as paraffinum liquidum, which is a very highly refined mineral oil used in cosmetics and for medical purposes. We performed transmission measurements and found a quasi-flat dispersion curve for our two samples with $n = 1.465$ for the liquid (cf., Fig. 2) and $n = 1.511$ for wax, a solid form of paraffin we also characterized. The spectroscopic analysis showed a very low extinction coefficient for all the investigated bandwidths (less than 310^{-3} up to 3 THz).

To experimentally illustrate the benefits of the immersion of the samples in the considered liquids, we tested two different objects: a Teflon cylinder with a 5.6 mm diameter and a HDPE prism with an angle of 60° and a 10 mm base (cf., Fig. 3). We positioned the samples inside a PE box at the focus point of the THz beam, which was found by the knife edge technique or using a pinhole and monitoring the total transmitted intensity. It also gave us access to the intensity distribution in the space and the Rayleigh length for all frequencies. Then they were inserted under dry air condition and raster scanned in both X and Y directions, with a scanning step of 0.5 mm. Knowing the sample shapes and acquisition device properties, we thus exacerbated the refraction effect for transmission images at this resolution.

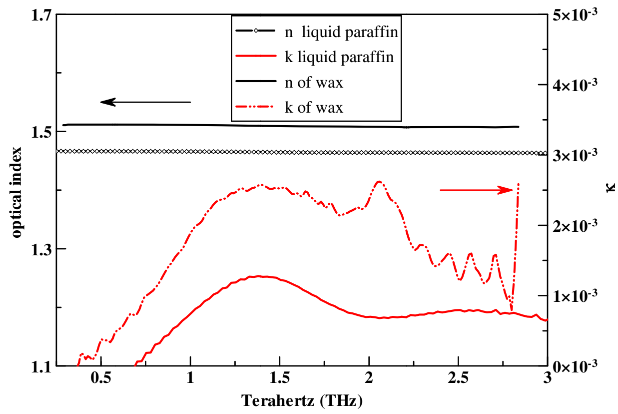

Fig. 2. Complex optical index of liquid paraffin and wax.

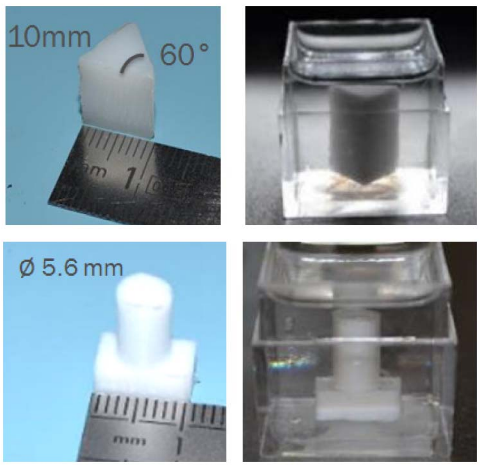

Fig. 3. Samples under investigation. Top pictures: (left) a polyethylene prism in air and (right) in paraffin. Bottom pictures: (left) a Teflon cylinder in air and (right) in paraffin.

4. RESULTS AND DISCUSSION

First, we will discuss the THz time domain data obtained without index-matching liquid. From these values, we calculated the average attenuation ($A = \ln(1/t)$), where t is the transmission at the selected THz frequency for each horizontal slice through a cross-section of the sample. In the case of the prism sample, the ridge was set in front of the emitter. The most imperative parameter to perform a 3D tomography analysis is to get the real thickness of the sample, which can be affected by the absorption coefficient. The latter determines how far into a material a particular wavelength can penetrate before it is absorbed. In the particular case of a nondispersive material and when the absorption is low (which is the case with PE), the intensity of the transmitted beam is directly linked with the thickness. Consequently, the simple analysis of the FFT amplitude of the transmitted beam correlated with its thickness and offered an idea about the shape of the sample.

For other material, a complete extraction of the dielectric function was necessary. In our work, we sought to evaluate the real dimensions of the object when it suffered from refraction losses (i.e., nonflat interfaces with respect to the propagating beam). Next, we compared the transmitted amplitude for some typical frequencies and analyzed their intensity dispersion as a function of the position, with and without the index-matching liquid. The different intensity variation then reflected the apparent optical thickness.

Figure 4 shows the typical FFT amplitude for selected images at 1.4 THz for (a) the cylinder and (b) the prism. We observe several artifacts. Boundary effects occurred because of the abrupt refractive index change at the interface between the sample and the surrounding media, as well as the Fresnel reflection losses [19]. These distortions, present for all frequencies, hampered a coherent measurement of the sample and would induce errors in any further processing (3D tomographic or time-of- flight reconstructions, for instance) [20].

The second important drawback was located at the center of the devices, which acted as a lens for the THz beam. Slightly visible in the prism due to the important curvature at the edge of the ridge, this effect was more critical for a cylinder sample, where the convolution of the Gaussian profile and the reflection area gave rise to a bright line localized in the middle of the projection image. This is more and more crucial when we displayed an amplitude image at low frequency since the spatial extension of the Gaussian distribution spreads out when the frequency decreases. This is clearly exemplified in Fig. 4(a), where the bright area extends in the center of the cylinder. Finally, the third consequence of the interaction of the THz beam with a nonparallel interface is the presence of multipeaks in the transmitted signal [12]. In Fig. 4(c), which represents a temporal transmitted signal near the second ridge of the prism, data contain multiple peaks with maximum intensity 25 times smaller than the reference signal.

This observation shows the strong refraction effect at this spatial position. Moreover, the presence of multiple peaks made it difficult to choose the correct peak for time delay measurement, which made phase imaging quite complicated. For the cylinder case, the distortion of the temporal data was less pronounced but the amplitude was still low. Then, it was impossible to render a correct shape of the sample by phase analysis. Moreover, the amplitude image was biased since the record was quite homogeneous with a very low level (due to the prominence of the reflection and refraction effects). That does not reveal the triangular shape and the intensity profile expected in that case.

Figure 5 presents the results obtained when the samples were immersed into the index-matching liquid, at the same frequency as on Fig. 4. We observed the same behavior for different available frequencies in the experiment. Since the reflection coefficients and losses for the both interfaces between the sample and the medium strongly depended on the index difference, the total recorded transmitted signal was greatly enhanced when we used an index value close to the sample one. Moreover, the multipeak occurrences were greatly reduced, which allowed us to investigation the thickness using transmitted phase analysis. Note that time domain data is not shown, but is identical to the reference signal with a small temporal shift and an amplitude diminution due to the weak index mismatch and the low absorption of PE.

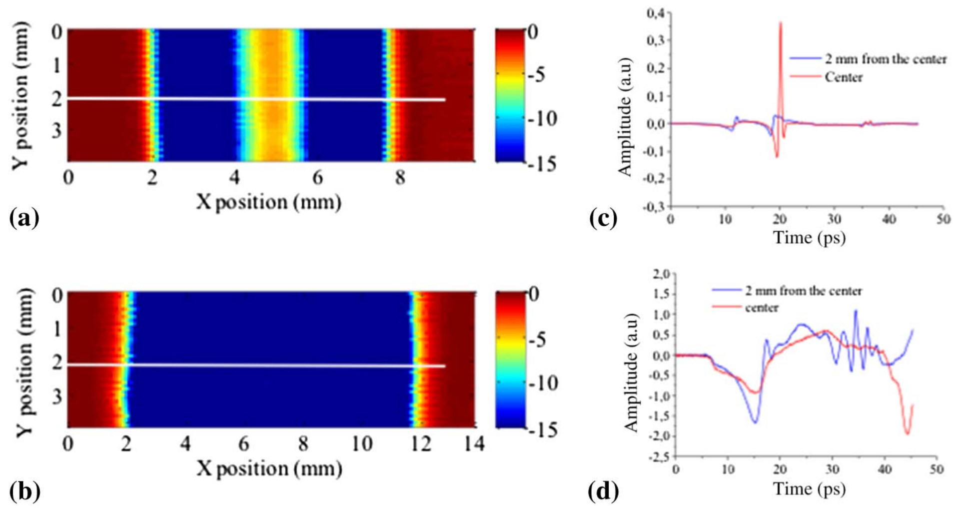

Fig. 4. FFT amplitude images of the PE cylinder (a) and prism (b) at 1.4 THz , temporal data at the center and 2 mm besides cylinder (c) for the prism (d).

The "lens effect" was still visible on the triangular shape, but was largely attenuated in the case of the cylinder [cf., Fig. 4(a)]. Conversely, the effect of blurring the boundaries was only prominent in the case of the cylinder. Moreover, the cylinder seemed transparent at 1.4 THz, which is more coherent with the PE sample. The refraction loss was clearly the main limiting phenomenon. We have also presented an intensity plot profile obtained at the 2 mm position for both samples [Figs. 5(c) and 5(f)]. More than 40 dB of the intensity has been recovered, leading to a profile in good agreement with the theoretical calculation obtained with the Beer–Lambert law and supposing that the absorption coefficient is also in agreement, without taking into account refraction and finite size beam effect [19], Figs. 5(a) and 5(b).

In Fig. 6, we simulated a geometrical optical ray tracing approach to quantify the optical effects of refraction and reflection, depending upon the properties of the samples and the different geometries. We performed the simulations and only focused on the Rayleigh zone of our THz time domain spectroscopy system. The ray tracing model considered the refraction effect and we neglected the absorption and scattering effects. Then we compared the PE prism and Teflon cylinder when they were inserted in the empty polymer box or filled with the liquid paraffin. Figure 6 shows the optical effects at

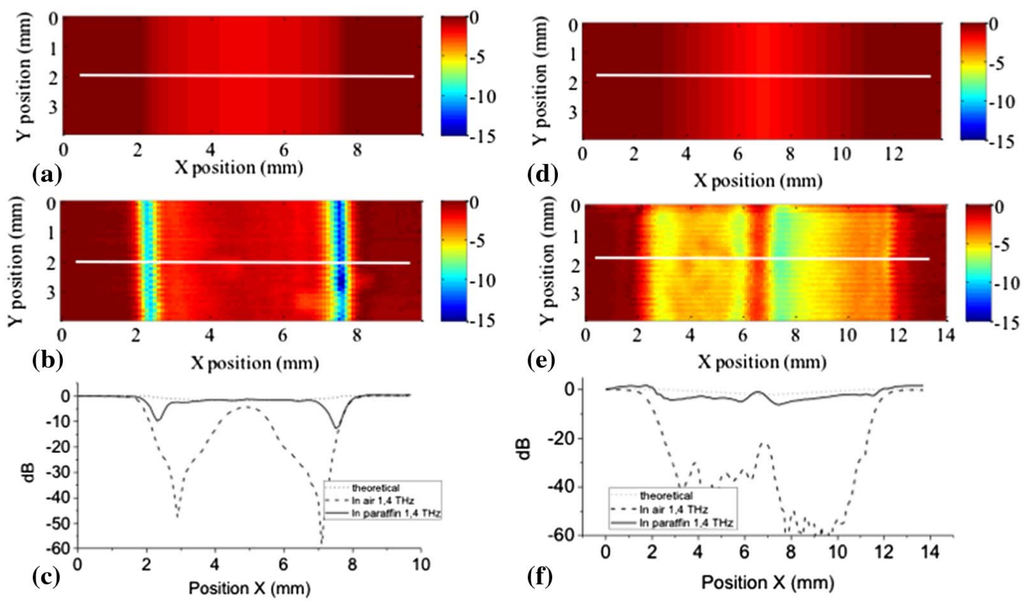

Fig. 5. Theoretical absorption profiles without refraction effect for the cylinder (a) and the prism (d), FFT amplitude images of the cylinder (b) and PE prism (e) immersed in liquid paraffin at 1.4 THz and intensity plot profiles of the cylinder. (c) and prism (f) in dB, at the 2 mm position, theoretical profile is added.

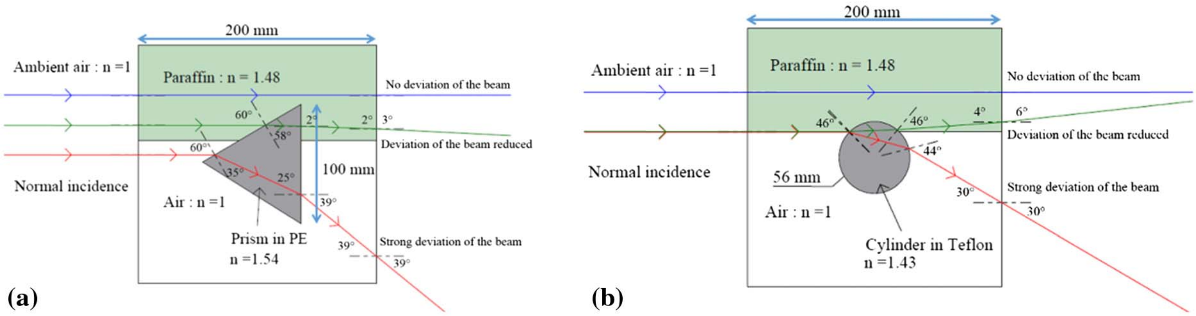

Fig. 6. Comparison of ray tracing through (a) the PE prism and (b) the Teflon cylinder surrounded either by the air (white) or by the paraffin (green). The blue ray passes straight through the medium only, the red one undergoes a strong deviation after passing through the sample, whereas the deviation of the green one is strongly limited by the index matching.

the refractive surfaces, where we compared ray tracing through (a) the PE prism and (b) the Teflon cylinder surrounded either by the air (white) or the paraffin (green). The blue ray passed straight through the sample immersed in liquid. For the prism, the deviation was 3°. With the cylinder we obtained only 6°. The red one underwent a strong deviation after passing through the sample, between 30° and 40° for the both samples (whereas the deviation of the green one was strongly limited by the index matching).

These simulation results could help a researcher choose the optimized numerical aperture of the collecting optics to reduce refraction losses since sensors are generally a mono pixel positioned prior to inserting the sample in the beam trajectory.

Many researchers use the very good depth penetration of the THz beam to implement a contactless thickness measurement [21,22]. For the THz radiation, the beam propagation remains straight, eventually due to matching the condition propagation into the medium presenting no dispersion in the THz bandwidth. In that case, the time delay between a reference pulse into the liquid and the transmitted signal is the optical thickness given by

$$C\Delta t = (n_m - n_s)d, \tag{1}$$

where c is the velocity of light, Δt is the time offset between reference and transmitted signals, d is the thickness at the measurement position, and n_m and n_s are the group refractive index of the medium and the sample, respectively. By mapping in x and y positions and after Fourier transformation of temporal data, we calculated the local thickness d by

$$d(x,y) = \frac{\Delta\varphi(x,y,\omega)\cdot c}{(n(\omega)_{\text{sample}} - n(\omega)_{\text{medium}})\cdot\omega}. \tag{2}$$

$\Delta\varphi(x,y,\omega)$ is the phase difference at ω between the beam traveling through the liquid and through the sample. In the experimental case, we first must perfectly characterize the empty box dimensions and the dielectric response, which can be easily performed by time domain spectroscopy [23]. Then, we measure the transmitted signal for the sample positioned into the box to evaluate the real optical thickness of the liquid. We can at least subtract the phase contribution of the polymer box and paraffin.

Figure 7(a) presents the variation of the unwrapped phase difference for different frequencies for the prism sample. The slopes were quite linear and demonstrated the possibility to sense the real shape of the sample despite the refraction loss. Knowing the dielectric response of the liquid and the sample material (the optical index of polyethylene is 1.54 for all THz frequencies), we could reconstruct the third dimension precisely and assess the presence of defects inside the sample even if it had a complex curvature (leading to the predominance of refraction losses in air). Quantitatively, we compared the height of the triangle of the prism extracted from phase at different

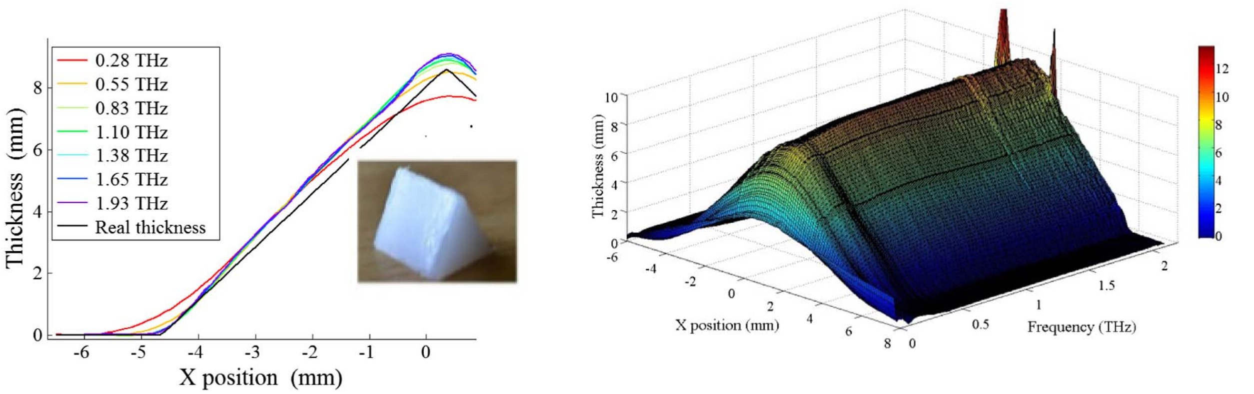

(a) (b)

Fig. 7. (a) Phase for different frequencies. (b) Phase-imaging reconstruction of the prisms as function of the frequency.

frequencies with the measured thickness of the prism with a caliper. In Fig. 7(b), we measured the thickness of the prism, which corresponded to the stacking of Fig. 7(a) from 0.1 to 2 THz.

We observe a spreading of the maximum thickness as a function of the frequency, with more a pronounced deviation at lower frequencies. The slopes of the sample are well reproduced independent of the frequency. It is clear that the extracted height from phase increases with the frequency and then converges until 9.3 mm from 1 THz. Moreover, the measured dimension of the sample and the deviation of the extracted thickness are mainly linked to the finite beam size of the THz beam and the propagation effect. This method gives results in the order of magnitude for the thickness of the prism, but overestimated the thickness by 8.1%. Assuming Gaussian beam propagation for all frequencies, and because of the important angle of refraction, experimental artifacts from the frequency-dependent waist size were the major source of errors. Using our setup, we achieved and measured beam waists in the range of 1–2 mm. In the frequency domain (between 1 and 2 THz), where we measured a constant thickness of the prism, these convolved effects tend to decrease the measured height. For example, Fig. 8 is the 3D reconstruction of the PE prism inserted in liquid paraffin. We convert the

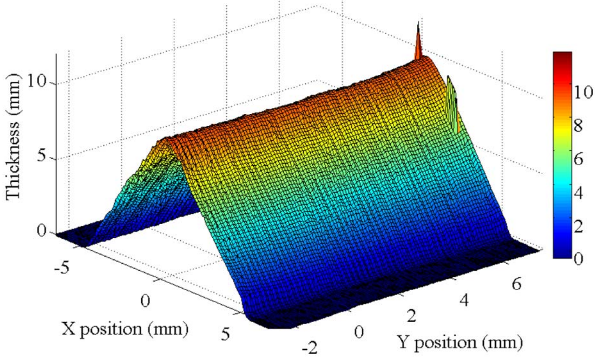

Fig. 8. Reconstructed PE prism at 2 THz.

phase information into depth (z axis) by applying the different steps described previously.

Quantitatively, the Fresnel reflection losses could be included using the power reflection coefficient

$$R = \left(\frac{(n_i \cos\theta_i - n_t \cos\theta_t)}{(n_i \cos\theta_i + n_t \cos\theta_t)}\right)^2, \tag{3}$$

where n_i, n_t, θ_i, and θt are the refractive index of the incident medium, the refractive index of the transmitted medium, incidence, and transmitted angle, respectively. Using both Snell's law and Eq. (2) for both the air sample and sample air interfaces and replacing the air by liquid paraffin tremendously reduced the reflection losses at the two boundaries. For instance, the reflection coefficient r varied from 0.2 down to 0.02 while the attenuation loss in the sample could be negligible. As a consequence, the major part of the initial signal was transmitted and did not undergo the refraction effect. Then, the initial temporal beam was weakly affected and phase analysis was easily feasible.

Concerning the cylinder, a complete calculation algorithm of artifacts coming from refraction effect was implemented to correct distortion in the THz projection data [19]. Since the steering effect was the more noticeable artifact, they successfully recovered the physical intensity profile after developing a dedicated numerical correction procedure.

Figure 9 shows the intensity projection with and without paraffin at two frequencies (1 THz and 2 THz, respectively). We also provided an intensity plot profile. Clearly, the intensity profile with paraffin correctly reproduces the major part of the cylinder without any artifact or correction. The structural feature at the interface, however, is strongly attenuated, but still remains. We have also reported the variation of internal intensity with frequency, demonstrating the anticorrelation between the lens effect and wavelength. When we apply the 10%–90% criterion for the edge detection, the measured width was 5.8 mm, which gives a ~4% error with respect to a 5.6 mm measured with a caliper. With the same approach, due to the index-matching immersion of the sample, the unwrapped phase difference for different frequencies gives access to the real shape of the cylinder. For lower frequencies, the beam waist

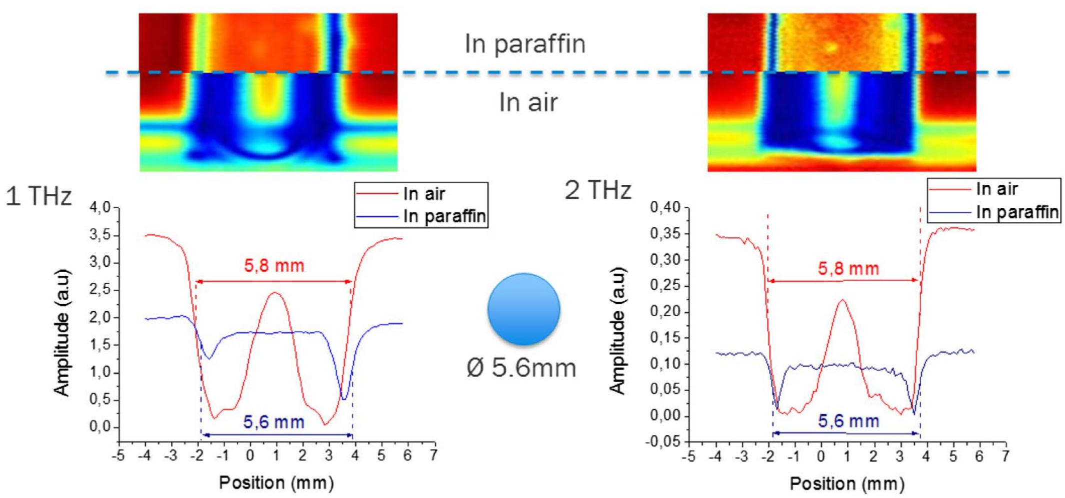

Fig. 9. Superposition of FFT amplitude images at 1 and 2 THz with and without paraffin for the cylinder sample and intensity plot profiles.

effect convolved with the geometry effects led to a systematic under-evaluation (varying with the frequency) of the measured diameter (between 5 and 5.4 mm).

THz imaging is often rivaled by ultrasound testing. The scanning acoustic microscope (SAM) was established as a tool to study the internal microstructure of nontransparent solids or biological materials. In acoustic microscopy, ultrasound waves image a sample, and the contrast in reflection provides a map of the spatial distribution of the mechanical properties. The lateral resolution is dependent on the frequency of the acoustic waves and, at best, is about 0.75 μm with 2 GHz transducers. Like terahertz imaging or tomography, the scanning acoustic microscope is a sequential imaging system in which a piezoelectric transducer emits a focused ultrasound beam that propagates through a necessary fluid to the sample.

The beam is scattered by the sample, and the scattered ultrasound wave is then detected. The size of the focal spot is limited by diffraction. We acquired images when the acoustic microscope mechanically scanned a sample in a plane parallel to the sample surface. Accumulating images obtained at various depth positions allowed us to construct a 3D image. Identically, time-resolved acoustic microscopy improved the analysis for quantitative measurement. Similarly, the time of flight for different pulses and their amplitudes identifies the elastic properties and attenuation of sound in the layer. Time-resolved images obtained by mechanical scanning along a line are called B-scans. Data and image processing allowed the image formation of subsurface defects and 3D objects, SAM are intensively used for NDT in microelectronics and medical applications.

THz radiations in some cases offer a great advantage over ultrasound because the THz region of the spectrum corresponds to a frequency in which many relevant molecular and lattice vibration and structural changes occur. It has transmission and reflection properties that are highly sensitive to the index of refraction n (ω) and absorption coefficient a (ω) in a huge spectral range rather than the mechanical properties. Also, THz techniques have been demonstrated with a high signal-to-noise ratio (SNR) of 500–10,000 and THz radiation also provides a possibility simultaneously acquire spectral, spatial, and temporal information with a time domain system. Moreover, THz radiation interacts with dielectric defects primarily by classical Mie scattering.

This approach allows a much simpler imaging setup. THz data may also be complementary to Raman spectroscopy because it also provides information on both high-frequency (just below IR) and low-frequency vibrational modes compared to a mono frequency response. At the very least, it is only for non-planar objects such as cylinders or samples, whereas a strong diffraction effect is observed, indicating that the use of an index-matching liquid could help to reduce artifacts. Art and heritage analysis techniques, for example, are important for restoration and conservation as well as for aeronautics, which could be analyzed by standard THz spectroscopy and imaging tools.

Depending on the surface and the shape of the studied samples, we can also use special optics to collect the refracted and transmitted beams to the detectors and then obtain only absorption as contrast parameter. In all cases, each technique presents advantages, drawbacks, and limitations for imaging the surface, sub-surface, and internal structure of an object. For a potential application, many experiments should be conducted with samples, understanding that there are some trade-offs such as the optimal wavelength to combine transparency, the resolution, and the ability to fairly image the sample.

5. CONCLUSION

During image acquisition, an important part of the THz beam is reflected, diffracted, and refracted at each interface because of the refractive index mismatch and reflection in the case of non-normal incidence. These phenomena cause severe artifacts for 2D imaging analysis and 3D rendering. To adapt the refractive index of the medium around a sample, we replaced the surrounding air with a liquid with an optimized refractive index and a low absorption over a large spectral THz bandwidth. We selected numerous nonpolar liquid n alkanes with their optical indexes ranging from 1.35 to 1.52, which is suitable for many compounds. This technique greatly reduced distortion at the edge and at the center of the samples.

The multiple peaks we observed in the temporal data after transmission through the sample were then reduced to a single peak, allowing phase retrieval. Phase imaging enhanced the reconstruction of complex shapes such as a prism or a cylinder and allowed more accurate measurement of the thickness. The boundary effect was significantly reduced, enabling us to correctly size the sample. We are encouraged by these results and believe they open the way to time-of-flight tomography of complex samples. When the sample internal and external structure geometry is more complicated, however, the multiple reflections and refractions of the THz radiations could overlap and scatter, making analysis more problematic.

Funding. Conseil Région D' Aquitaine.

Acknowledgment. We thank the Conseil Région D' Aquitaine for financial support in the framework of 3R3D project.

REFERENCES

1. J. Guillet, B. Recur, L. Frederique, B. Bousquet, L. Canioni, I. Manek-Hönninger, P. Desbarats, and P. Mounaix, "Review of terahertz tomography techniques," J. Infrared Millim. Terahertz Waves **35**, 382–411 (2014).
2. C. Jansen, S. Wietzke, O. Peters, M. Scheller, N. Vieweg, M. Salhi, N. Krumbholz, C. Jördens, T. Hochrein, and M. Koch, "Terahertz imaging: applications and perspectives," Appl. Opt. **49**, E48–E57 (2010).
3. B. Ferguson, S. H. Wang, D. Gray, D. Abbott, and X. C. Zhang, "Towards functional 3D T-ray imaging," Phys. Med. Biol. **47**, 3735–3742 (2002).
4. W. L. Chan, J. Deibel, and D. M. Mittleman, "Imaging with terahertz radiation," Rep. Prog. Phys. **70**, 1325–1379 (2007).
5. B. Recur, J.-P. Guillet, I. Manek-Hönninger, J.-C. Delagnes, W. Benharbone, P. Desbarats, J.-P. Domenger, L. Canioni, and P. Mounaix, "Propagation beam consideration for 3D THz computed tomography," Opt. Express **20**, 5817–5829 (2012).
6. J. Pearce, H. Choi, D. M. Mittleman, J. White, and D. Zimdars, "T-ray reflection computed tomography," in *Conference on Lasers and Electro-Optics (CLEO)*, Baltimore, Maryland, USA, 22 May 2005.
7. V. P. Wallace, E. MacPherson, J. A. Zeitler, and C. Reid, "Three-dimensional imaging of optically opaque materials using nonionizing terahertz radiation," J. Opt. Soc. Am. A **25**, 3120–3133 (2008).

8. F. Ospald, W. Zouaghi, R. Beigang, C. Matheis, J. Jonuscheit, B. Recur, J.-P. Guillet, P. Mounaix, W. Vleugels, and P. V. Bosom, "Aeronautics composite material inspection with a terahertz time-domain spectroscopy system," Opt. Eng. **53**, 031208 (2014).
9. J. A. Zeitler, P. F. Taday, D. A. Newnham, M. Pepper, K. C. Gordon, and T. Rades, "Terahertz pulsed spectroscopy and imaging in the pharmaceutical setting–a review," J. Pharm. Pharmacol. **59**, 209 (2007).
10. D. M. Mittleman, R. H. Jacobsen, and M. C. Nuss, "T-ray imaging," IEEE J. Sel. Top. Quantum Electron. **2**, 679–692 (1996).
11. J. Takayanagi, H. Jinno, S. Ichino, K. Suizu, M. Yamashita, T. Ouchi, S. Kasai, H. Ohtake, H. Uchida, and N. Nishizawa, "High-resolution time-of-flight terahertz tomography using a femtosecond fiber laser," Opt. Express **17**, 7533–7539 (2009).
12. E. Abraham, A. Younus, C. Aguerre, P. Desbarats, and P. Mounaix, "Refraction losses in terahertz computed tomography," Opt. Commun. **283**, 2050–2055 (2010).
13. B. Ferguson, S. H. Wang, D. Gray, D. Abbot, and X. C. Zhang, "T-ray computed tomography," Opt. Lett. **27**, 1312–1314 (2002).
14. Y. S. Jin, G. J. Kim, and S. G. Jeon, "Terahertz dielectric properties of polymers," J. Korean Phys. Soc. **49**, 513–517 (2006).
15. M. Naftaly and R. E. Miles, "Terahertz time-domain spectroscopy for material characterization," Proc. IEEE **95**, 1658 (2007).
16. J. E. Pedersen and S. R. Keiding, "THz time-domain spectroscopy of non polar liquid," IEEE J. Quantum Electron. **28**, 2518–2522 (1992).
17. J. Laib and D. Mittleman, "Temperature-dependent terahertz spectroscopy of liquid n-alkanes," J. Infrared Millim. Terahertz Waves **31**, 1015–1021 (2010).
18. Y. Danten, M. Besnard, J.-C. Delagnes, and P. Mounaix, "Far infrared absorption and terahertz time domain spectroscopy of liquid CS2: experiments and molecular dynamics simulation," Appl. Phys. Lett. **92**, 214102 (2008).
19. S. Mukherjee, J. Federici, P. Lopes, and M. Cabral, "Elimination of Fresnel reflection boundary effects and beam steering in pulsed terahertz computed tomography," J. Infrared Millim. Terahertz Waves **34**, 539–555 (2013).
20. B. Recur, H. Balacey, J. Bou Sleiman, J.-B. Perraud, J.-P. Guillet, A. Kingston, and P. Mounaix, "Ordered subsets convex algorithm for 3D terahertz transmission tomography," Opt. Express **22**, 23299 (2014).
21. T. Yasui, T. Yasuda, K.-I. Sawanaka, and T. Araki, "Terahertz paintmeter for noncontact monitoring of thickness and drying progress in paint film," Appl. Opt. **44**, 6849–6856 (2005).
22. H. Zhong, J. Xu, X. Xu, Y. Tao, R. Reightler, E. Madaras, and Z. Xi-Cheng, "Nondestructive defect identification with terahertz time-of-flight tomography," IEEE Sens. J. **5**, 203–208 (2005).
23. L. Duvillaret, F. Garet, and J. L. Coutaz, "Highly precise determination of optical constants and sample thickness in terahertz time-domain spectroscopy," Appl. Opt. **38**, 409–415 (1999).